IBRO Neuroscience Reports 11 (2021) 29–41

Contents lists available at ScienceDirect

IBRO Neuroscience Reports

journal homepage: www.sciencedirect.com/journal/IBRO-Neuroscience-Reports

Visual deprivation induces transient upregulation of oligodendrocyte progenitor cells in the subcortical white matter of mouse visual cortex

Hyeryun Shin [a], Hideki Derek Kawai [b,*]

[a] Department of Bioinformatics, Graduate School of Engineering, Soka University, Hachioji, Tokyo 192-8577, Japan
[b] Department of Biosciences, Graduate School of Science and Engineering, Soka University, Hachioji, Tokyo 192-8577, Japan

ARTICLE INFO

Keywords:
Glia
Sensory cortex
Visual deprivation
White matter

ABSTRACT

Sensory experience influences proliferation and differentiation of oligodendrocyte progenitor cells (OPCs). Enhanced sensorimotor experience promoted the lineage progression of OPCs and myelination in the gray matter and white matter (WM) of sensorimotor cortex. In the visual cortex, reduced experience reportedly delayed the maturation of myelination in the gray matter, but whether and how such experience alters the subcortical WM is unclear. Here we investigated if binocular enucleation from the onset of eye opening (i.e., P15) affects the cell state of OPCs in mouse primary visual cortex (V1). Proliferative cells in the WM declined nearly half over 3 days from postnatal day (P) 25. A 3-day BrdU-labeling showed gradual decline in proliferation rates from P19 to P28. Binocular enucleation resulted in an increase in the cycling state of the OPCs that were proliferated from P22 to P25 but not before or after this period. This increase in proliferative OPCs was not associated with lineage progression toward differentiated oligodendrocytes. Proliferative OPCs arose mostly due to symmetric cell division but also asymmetric formation of proliferative and quiescent OPCs. By P30, almost all the proliferated cells exited the cell cycle. Maturing oligodendrocytes among the proliferated cells increased at this age, but most of them disappeared over 25 days. The cell density of the maturing oligodendrocytes was unaffected by binocular enucleation, however. These data suggest that binocular enucleation transiently elevates proliferative OPCs in the subcortical WM of V1 during a specific period of the fourth postnatal week without subsequently affecting the number of maturing oligodendrocytes several days later.

Introduction

The subcortical white matter (WM) contains projecting axons that mediate the transmission of neural information and myelin that wraps around them for proper conduction of electrical impulses. Since myelin provides structural and functional modification of axons, while controlling the speed and timing of electrical conduction of neural information, it would be important to understand how oligodendrocytes (OLs) develop to form mature neural circuits. Oligodendrocyte progenitor cells (OPCs) are the progenitor cells of myelin-forming OLs. OPCs preside in the WM with about 50% more density than in the gray matter (GM) (Dawson et al., 2003). These OPCs proliferate to self-renew and to differentiate into OLs (Rivers et al., 2008; Guo et al., 2009; Kang et al., 2010; Young et al., 2013; Nishiyama et al., 2014). The rate of this OPC development is faster in the WM than in the GM (Simon et al., 2011). Significance of this property of OPCs remains to be discovered.

OPC proliferation is under the influence of axonal activities. OPC proliferation increased when axonal conduction was locally inhibited by the voltage-dependent sodium channel inhibitor tetrodotoxin in adult corpus callosum in vivo (Gautier et al., 2015). Such increase in OPCs was also detected in the GM of the barrel field of the somatosensory cortex when whiskers were removed at birth, preventing the sensory evoked inputs reaching the cortex (Mangin et al., 2012; Hill et al., 2014). In contrast, when neuronal activity was enhanced, OPC proliferation decreased as demonstrated in dorsal root ganglion in vitro (Stevens et al., 2002). Thus, neuronal activity loss appears to increase the number of OPCs, while activity gain decreases it. However, the story is not simple. Enhanced neuronal activity increased, not decreased, OPC proliferation in the corticospinal tract and the subcortical WM of adult motor cortex (Li et al., 2010; Gibson et al., 2014), suggesting the cortical region-dependence of OPC proliferation. The driving force for the increased OPC proliferation may be a homeostatic compensation of the OPC loss due to the allocation of divided OPCs to differentiation (Hughes et al., 2013; Xiao et al., 2016). In the subcortical WM of the

* Correspondence to: Faculty of Science and Engineering, Soka University, Hachioji, Tokyo 192-8577 Japan.
E-mail address: kawai@soka.ac.jp (H.D. Kawai).

https://doi.org/10.1016/j.ibneur.2021.06.004
Received 6 May 2021; Received in revised form 13 June 2021; Accepted 23 June 2021
Available online 28 June 2021
2667-2421/© 2021 The Author(s). Published by Elsevier Ltd on behalf of International Brain Research Organization. This is an open access article under the CC BY-NC-ND license (http://creativecommons.org/licenses/by-nc-nd/4.0/).

visual cortex, the nature of OPC proliferation and differentiation and their activity dependence are largely unknown.

Recently, we have found that binocular enucleation (BE) at the time of eye opening on P15 increased OPC undifferentiation during a specific developmental period and later enhanced differentiation in the GM of mouse primary visual cortex (V1). BE increased OPC proliferation as detected by once-a-day injection of 5′-bromo-2-deoxyuridine (BrdU) from P22 to P25 (P22–25) as compared to P19–22 or P25–28. This increased proliferation was associated with a reduction of differentiation and an elevation of proliferative cells expressing Ki67, a nuclear protein expressed during the cell cycle (Gerdes et al., 1984; Miller et al., 2018), in the bottom layer of the cortex. Interestingly, maturation increased 25 days later. Our data suggested that P22–25 is a particularly sensitive period for neural activity-dependent OPC proliferation. Here, in this report, we examine developmental changes of oligodendrocyte lineage cells and BE effects on OPC proliferation and differentiation in the subcortical WM of V1 around this peculiar period.

Materials and methods

Animals

All experiments used C57BL/J mice (postnatal days (P) 15–50) housed in a vivarium with 12 h light/12 h dark cycle. All animal procedures followed the Guide for the Care and Use of Laboratory Animals (US National Research Council Committee, 2011), and were approved by the Institutional Animal Care and Use Committee at Soka University.

Binocular enucleation was conducted as described previously (Karlen and Krubitzer, 2009; Aerts et al., 2014) with modification and has been approved by the IACUC. Briefly, mice at P15 (the first day of eye-opening) were anesthetized with 2% isoflurane (Cat# 008313, Intervet) with a gas mixture of 1.0 L/min O_2 and 1.5 L/min N_2O via a mask over the nose while maintaining the body temperature at 37 ℃. Then, following the application of 2% lidocaine (Cat# 125-05681, Wako) on and around eyelids to anesthetize peripheral tissues, eye was opened, and an eyeball was lifted with forceps, optic nerves were occluded along with blood vessels for a while and dissected using a surgical scissor, and an eyeball was then removed from the orbit. After enucleation, a piece of sterile Gelfoam (Pfizer) was inserted inside the orbit, the eyelid was closed, and 2% lidocaine or 0.25% bupivacaine (LKT laboratories, USA) was applied on the eyelid. An opposite eye was subsequently removed as above. This binocular enucleation procedure typically took under 5 min. For sham control, mice were subjected to the same surgical procedure except the eye removal procedure. Following the surgery, sham control and the enucleated mice were subcutaneously injected with 5 mg/kg of anti-inflammatory drug meloxicam (Metacam; Cat# M20812A-32, Boehringer Ingelheim) once daily for 3 days to relieve pain. Body temperature, heart rate, and respiration were continuously monitored throughout the surgery. The enucleated and sham control mice were returned to their mother and siblings in a cage with nesting materials after surgery. Animals were housed in a vivarium with 12 h light/12 h dark cycle and monitored daily to check the health of the animals. After weaning, mice were hand-fed (typically for 3–5 days) until they could feed off the feeder to ensure survival and minimize the impact of visual compromise. All the animals that undergone surgery survived without significant loss of body weight.

5′-bromo-2-deoxyuridine (BrdU, Cat# B5002, Sigma) was injected intraperitoneally (i.p.) to each mouse daily once at the dose of 100 mg/kg body weight for 3 days and at 2 h before sacrifice in the fourth day.

Immunofluorescence staining

Mice were anesthetized with urethane (1.0 g/kg, i.p.; Cat# U2500, Sigma) and xylazine (13 mg/kg, i.p.; Cat# X1251, Sigma) and transcardially perfused with ice-cold phosphate-buffered saline (PBS) followed by 4% (wt/vol) paraformaldehyde (Cat# 168-23255, Wako) in 0.1 M phosphate buffer (4% PFA) for 5 min depending on primary antibodies used. The brains were extracted and post-fixed in the same fixative for ~2 h at 4 °C. Free-floating coronal sections (40–50 μm thickness) were obtained using a vibratome (Cat# DTK-1000, Dosaka). The sections were permeabilized using a blocking solution (BS: 5% normal donkey or goat serum, 0.3% (vol/vol) Triton X-100 in PBS) for 2 h at room temperature. Primary antibodies (see below) were diluted in blocking solution and incubated overnight at 4 ℃, and secondary antibodies (typically at 1/500; see below) were diluted in BS and incubated for 1.5 h at room temperature. Cell nuclei were visualized by post-staining with Hoechst 33342 (3 μg/ml; Thermo Fisher). Stained sections were mounted with Vectashield Antifade Mounting Medium (Cat# H1000, Vector Laboratories).

For antigen retrieval of anti-Ki67 antibody, sections were heat-treated in a water bath for 30 min in sodium citrate buffer (pH 6.0) at 80 °C, cooled down to room temperature, and subsequently rinsed in PBS for 10 min several times. For BrdU staining, sections were pre-treated in 1 N HCl for 45 min at 37 ℃ to partially denature the doublet-stranded DNA, neutralized with 0.1 M borate buffer (pH 8.5) twice for 15 min, and then rinsed in PBS for 10 min several times. For further reaction for multiple staining, the sections were incubated in 4% PFA for 1 h at 4 °C after incubation of secondary antibody. For primary antibodies raised in mouse, sections were pretreated with the mouse-on-mouse immunodetection kit (MOM kit, Vector, BMK-2202) in 0.3% (vol/vol) Triton X-100 in PBS.

Primary antibodies were a rat monoclonal antibody against BrdU (clone BU1/75(ICR1), GeneTex Cat# GTX26326, RRID:AB_1081056; Abcam Cat# ab6326, RRID:AB_305426), mouse monoclonal antibodies against Nestin (clone rat-401, Millipore Cat# MAB353, RRID:AB_94911; DSHB Cat# Rat-401, RRID:AB_2235915), CNPase (Millipore Cat# MAB326, RRID:AB_2082608), and CD68 (clone ED-1, Millipore Cat# MAB1435, RRID:AB_177576); rabbit polyclonal antibodies against Ki67 (Leica Microsystems Cat# NCL-Ki67p, RRID:AB_44210), NG2 (Millipore Cat# AB5320, RRID:AB_91789), Olig2 (Millipore Cat# AB15328, RRID:AB_2299035), GFAP (Millipore Cat# AB5804, RRID:AB_2109645), and goat polyclonal antibodies against Olig2 (Santa Cruz Biotechnology, sc-19969, RRID:AB_2236477) and PDGFRα (R&D Systems Cat# AF1062, RRID:AB_2236897).

Secondary antibodies from Jackson ImmunoResearch Laboratories (West Grove, PA) were goat anti-rat IgG conjugated with DyLight405 (112-475-167, RRID:AB_2338314), goat anti-rabbit IgG conjugated with Alexa488 (111-545-144, RRID:AB_2338052), goat anti-mouse IgG conjugated Cy3 (115-165-166, RRID:AB_2338692), and goat anti-mouse Fcγ conjugated with Alexa647 (115-605-071, RRID:AB_2338909). Donkey anti-goat conjugated with Alexa555 (ab150130, RRID:AB_2715537) from Abcam. Goat anti-rat IgG conjugated with Alexa633 (A21094, RRID:AB_2535749) and goat anti-rabbit IgG conjugated with Alexa633 (A21070, RRID:AB_2535731) were from ThermoFisher.

Image acquisition and quantification

Low magnification image of cortical hemisphere was captured using a fluorescence microscope (Keyence BZ-9000) and images were automatically jointed using analyzer software (Keyence BZ Analyzer software, RRID:SCR_017205). Other images in the binocular region of V1 (V1b) were captured at 1 μm step using a confocal laser-scanning microscope (Leica TCS SP8) with HyD detectors. To define the analysis region of V1 in obtained images, we first drew a vertical line though the center of the ventral division of the medial geniculate nucleus (MGv) and drew a second line through the occipital cortex from the MGv at a 15° angle to the vertical line. This 15° angle line was assumed to run through V1 based on mouse atlas (Franklin and Paxinos, 2008). The regions of interest (ROI) for counting cells were a subcortical WM region delimited by the border between layer 6 and WM, and two parallel lines with each line separated by 400 μm medial and lateral from the 15° line. Consecutive five or six sections were used per mouse, and at least three

mice were used per group. Optical dissector was used to determine the number of positively labeled cells and analyzed using Fiji/ImageJ software (NIH, USA, RRID:SCR_002285).

Cells with fluorescence intensity above a defined threshold were considered immunopositive cells. For cell counting, the mean background fluorescence intensity was calculated by averaging at least five unstained locations on the same histological sections. Threshold intensity was defined as 3x SD of the mean background intensity in each section and subtracted from the measured intensity in ROI. Cell counting was performed blind to experimental conditions. The cell density (cells/10^6 μm^3) was computed by dividing cell counts with laminar volume obtained from 30 μm optical sections.

The distance between adjacent BrdU immunopositive nuclei was measured in three-dimensional optical sections. BrdU immunopositive cells were considered doublets when the distance between the centers of the nuclei was below 35 μm as described previously (Boda et al., 2015). In the case of apparent triplet or quadruplet of BrdU+ cells, the nearest pair was defined as doublets.

Statistical analyses

Statistical analyses between groups were carried out using Excel (Microsoft) and the R Project for Statistical Computing (RRID: SCR_001905). Single parameter comparisons were performed using the unpaired Student's *t*-test between two experimental groups and one-way ANOVA for 3 groups. Variabilities between group means for one factor or two factors were analyzed using one-way or two-way ANOVA tests, respectively. For the multiple comparison of independent variables, statistical significance was determined with the Tukey post hoc test among two or four groups/conditions. All statistical tests used the significance level (α) of 0.05. A probability of $p < 0.05$ was considered statistically significant. N values represent the number of mice used. Data and error bars are reported as mean ± standard error of the mean in all graphs.

Results

The nature of proliferative cells in the subcortical white matter in V1

We examined the cell states of proliferative cells in the subcortical white matter (WM) of the binocular region of V1 during the fourth postnatal week and beyond. Daily injection of BrdU for 4 consecutive days resulted in the labeling of proliferated cells in the WM (Fig. 1). Essentially all BrdU+ cells were immunopositive for Olig2 and NG2 on

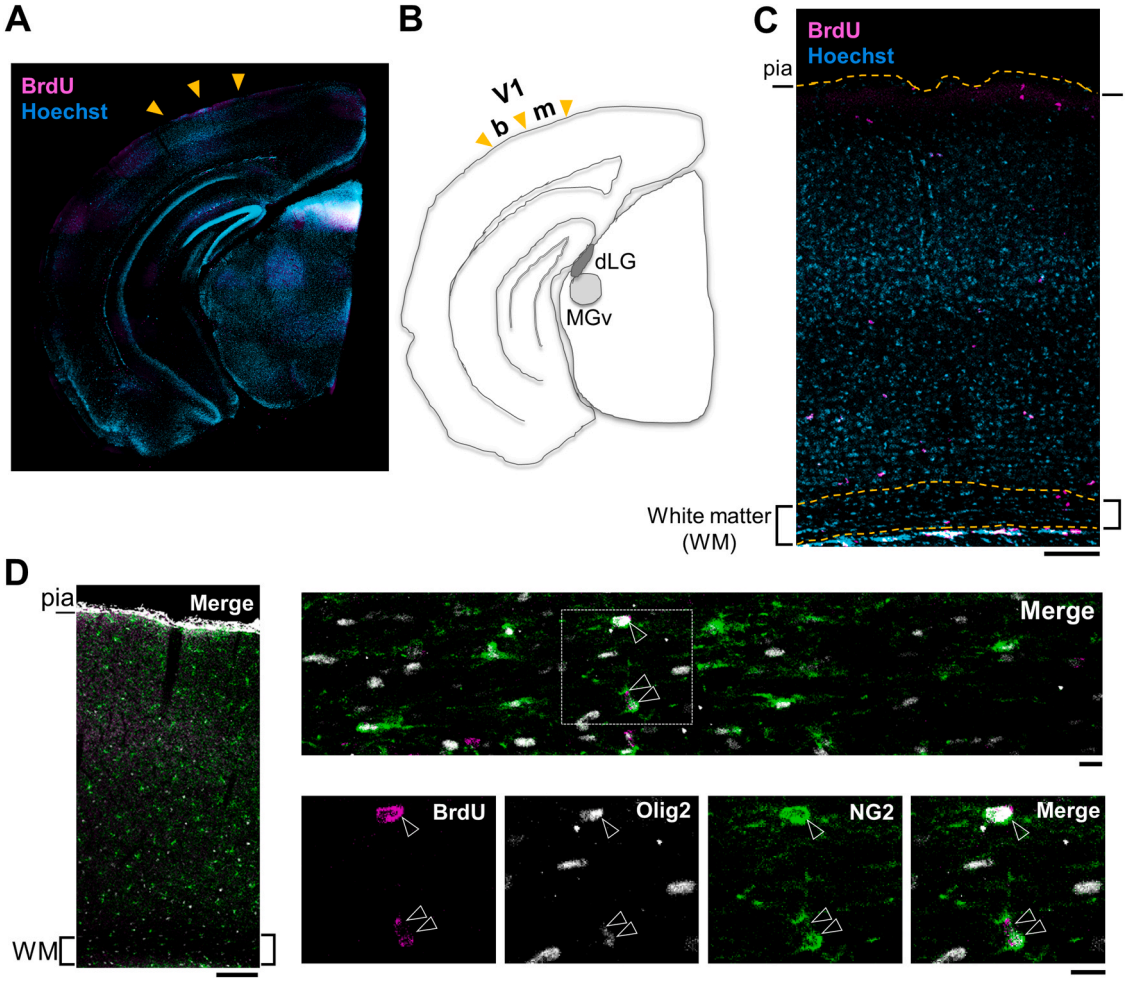

Fig. 1. Location of analysis area and BrdU-labeled cell type on P25. A. A representative low magnification image of the cortical hemisphere of a P25 mouse coronal brain section labeled with Hoechst (cyan) and BrdU (magenta). Yellow arrowheads point to approximate borders of binocular region (left) and monocular region (right) of V1. B. A drawing of the image in A to indicate the location of the binocular region (b) and monocular region (m) of V1, the ventral division of medial geniculate nucleus (MGv) and the dorsal lateral geniculate nucleus (dLG). C. A magnified image of the binocular region of V1 used for cell density analysis. Scale bar: 100 μm. D. A binocular region of mouse V1 (left) and a magnified image of the subcortical WM (top right). Magnified image of a boxed area (bottom right) immunostained against BrdU (magenta), Olig2 (gray), NG2 (green) and overlaid (Merge). Scale bars: 100 μm. (For interpretation of the references to color in this figure legend, the reader is referred to the web version of this article.)

P25 (Fig. 1D, 96.1 ± 1.4%, N = 6), suggesting that the proliferated cells are oligodendrocyte lineage cells (Dimou et al., 2008). Monitoring proliferative cells using immunostaining against Ki67 (Fig. 2A, B) indicated that the cell densities of proliferative cells in the WM of control mice were similar between P22 and P25, but they declined sharply to about a half within 3 days from P25 to P28 (one-way ANOVA, $F(2, 15) = 6.18$, $p = 0.011$ Tukey-Kramer post-hoc test, P25 vs. P28, $p = 0.00094$) and continued to decline nearly another half over 3 weeks from P28 to P50 (Fig. 2C). The sharp decline from P25 to P28 could be due to the decline of proliferation or a developmental cell transition from a cell cycling state to a cell cycle-exited state.

To explore this, we first examined proliferation rates by labeling oligodendrocyte lineage cells with the 4-day BrdU injection from P19 to P22 (P19–22), P22 to P25 (P22–25), or P25 to P28 (P25–28) followed by immunolabeling against BrdU as well as Ki67. The cell densities of BrdU+ cells appeared to decrease from P19–22 to P25–28 (Fig. 2D). The decrease in the proliferation rates from P22–25 to P25–28 was 4.4 cells/10^6 μm^3, which might contribute to the Ki67+ cell density loss from P25 to P28 (i.e., 6.0 cells/10^6 μm^3). Indeed, the proliferation rates of BrdU+Ki67+ cells decreased about 2.2 cells/10^6 μm^3 from P22–25 to P25–28 (Fig. 2E), which is more than one-third of the Ki67+ cell loss. Thus, the Ki67+ cell loss likely involves the decline of proliferation rates.

Despite the decrease of BrdU+Ki67+ proliferative cells from P22–25 to P25–28, there was no corresponding increase in BrdU+Ki67- cells (Fig. 2F). The proportions of Ki67- cells at any of the three periods remained similar (73% for P19–22, P71% for P22–25%, and 78% for P25–28). Combined with the above data, the results suggest that there was a decline of cell proliferation and a proliferated cell loss from P25 to P28 without clear change in the proportion of cell states among the three proliferation periods in control mice.

We next examined if the loss of Ki67+ cells involved a cell state change of proliferated cells by examining the destiny of P22–25 BrdU+ cells (Fig. 3). We stopped injecting BrdU at P25 and sacrificed animals 5 days later. The traced BrdU+ cells at P30 indicated about 28% loss of BrdU+ cells from P25 (Fig. 3A). Interestingly, the cell density of BrdU+Ki67+ cells in control mice almost disappeared fully on P30 (Fig. 3B). The extent of the BrdU+Ki67+ cell loss from P25 to P30 was about 4.8 cells/10^6 μm^3, which could account for some of the loss of Ki67+ cell densities seen from P25 to P30 (Fig. 2C; ~5.8 cells/10^6 μm^3 in control). Meanwhile, BrdU+Ki67- cell densities remained similar between P25 and P30 (Fig. 3C). These results suggest that the loss of Ki67+ cells involved the disappearance of the BrdU+ cells rather than the loss of Ki67 expression. Also, similar densities of the Ki67+ cells on P28 and P30 (Fig. 2C) suggest that the BrdU+ cell loss occurred within 3 days after proliferation.

P22-25 is a sensitive period for binocular enucleation-induced increase in proliferative OPCs

The effects of visual deprivation on the Ki67+ proliferative cells were assessed in the WM. Binocular enucleation (BE) at the time of eye opening on P15 resulted in generally higher cell densities of Ki67+ cells on P25 compared to control, though no significant difference was detected (Fig. 2C; unpaired Student's *t*-tests, $p = 0.13$). The Ki67+ cell density declined from P25 to P28 (one-way ANOVA, $F(2, 15) = 4.60$, $p = 0.028$) and continued to decline until P50 in BE mice as in control mice.

We then assessed if BE had any impact on proliferation rates and/or cell states. BE appears not to affect the BrdU+ proliferated cell densities for the three age periods (Fig. 2D; unpaired Student's *t*-tests, P19–22: $p = 0.95$, P22–25: 0.085, P25–28: $p = 0.86$), although the cell density for P22–25 appears slightly higher for BE over control. We found a significant difference in the proliferation rates between P22–25 and P25–28 (one-way ANOVA, $F(2, 15) = 7.96$, $p = 0.0044$, Tukey-Kramer post-hoc test, P22–25 vs. P25–28, $p = 0.0032$). Since the BrdU+ cell densities for P25–28 were similar between control and BE mice, P22–25 might be relatively a sensitive period for BE. In line with this assessment, BE significantly increased BrdU+Ki67+ cell density about 70% over control (Fig. 2E, unpaired Student's *t*-test, $p = 0.042$). Such increase was not found for P19–22 (unpaired Student's *t*-test, p = 042) nor P25–28 (unpaired Student's *t*-test, $p = 0.57$). Meanwhile, BrdU+Ki67- cell densities were not different between control and BE mice for the three BrdU-labeling periods (Fig. 2F, unpaired Student's *t*-tests, p19–22: $p = 0.68$, p22–25: $p = 0.50$, p25–28: $p = 0.70$). Thus, the BE-induced upregulation of BrdU+Ki67+ proliferative cells for P22–25 was not associated with the downregulation of Ki67- cell cycle-exited cells. These data suggest that P22–25 is a sensitive period for BE-dependent increase in newly proliferated, cell cycling OPCs without affecting the cell densities of the cell cycle-exited cells.

BE increased the proliferative OPCs without affecting cell cycle exit

Given that BE elevated the proliferative state of P22–25 BrdU+ OPCs, we speculated that OPC lineage is also affected by BE. We attempted to differentiate proliferative, quiescent, or differentiated states, utilizing immunofluorescent detection of Ki67 and nestin, an intermediate filament protein expressed in neural progenitors (Lendahl et al., 1990) (Fig. 4). Since nestin is expressed in undifferentiated oligodendrocyte lineage cells (Gallo and Armstrong, 1995; Guo et al., 2009; Rafalski et al., 2013; Dimou and Gallo, 2015), the cells that co-express Ki67 and nestin (Ki67+Nestin+) will be cycling cells, those that express nestin but not Ki67 (Ki67-Nestin+) will be cell cycle-exited immature cells, which potentially represent quiescent cells, and those that do not express both Ki67 and nestin (Ki67-Nestin-) will be oligodendrocyte-destined differentiated cells (Chen et al., 2017). Immunofluorescent images showed BrdU+ cells expressing Ki67 along with nestin around the nucleus in the cytosol, while others lacked Ki67 with or without nestin (Fig. 4A, B). Our examination of the proportion of BrdU+ cells in control mice indicates that about 30% was in the cell cycling state, about 40% was in the quiescent state, and about 30% was in the differentiated state (Fig. 4C). Notably, BE increased the cell density of Ki67+Nestin+ cycling cells. No significant increase was detected for presumptive quiescent and differentiated cells.

The increase in the cycling cells suggests an increase in the symmetric formation of proliferative cells. We assessed this by examining the symmetricity of cell division. BrdU+ cells were considered as sister cells or doublets when the distance between the centers of the two nuclei were within 35 μm (Boda et al., 2015). The cell density analysis indicated that BE increased symmetrically divided cycling (Ki67+Nestin+) doublets as well as Ki67+Nestin+/Ki67-Nestin+ asymmetric doublets. No other doublet types were affected. Thus, BE increases proliferative cells mostly symmetrically and, to lesser extent, asymmetrically without affecting the cell cycle exit.

BE increases OPCs without promoting lineage progression toward maturing OLs

We next examined if BE altered oligodendrocyte lineage progression using conventional oligodendrocyte lineage biomarkers (Fig. 5). The P22–25 BrdU+ cells were co-labeled with NG2 and nestin. NG2 is expressed mainly in OPCs and progressively degraded during differentiation, while nestin is expressed in both glial progenitor cells (GPCs) and OPCs but not in maturing OLs (Fig. 5A; Ghoumari et al., 2005; Reviewed in Schumacher et al., 2012; Kremer et al., 2016). Therefore, NG2-Nestin+, NG2+Nestin+, NG2+Nestin-, and NG2-Nestin- cells may be considered as GPCs, OPCs, early-differentiated oligodendrocytes (pre-oligodendrocytes or pre-OLs), and OLs, respectively. The analysis shows that OPCs and pre-OLs were the two major populations with nearly equal cell densities in control mice (Fig. 5C). BE appears to increase OPCs about 50%, while it decreases pre-OLs about 40%.

We then carried out the doublet analysis to examine the cell division

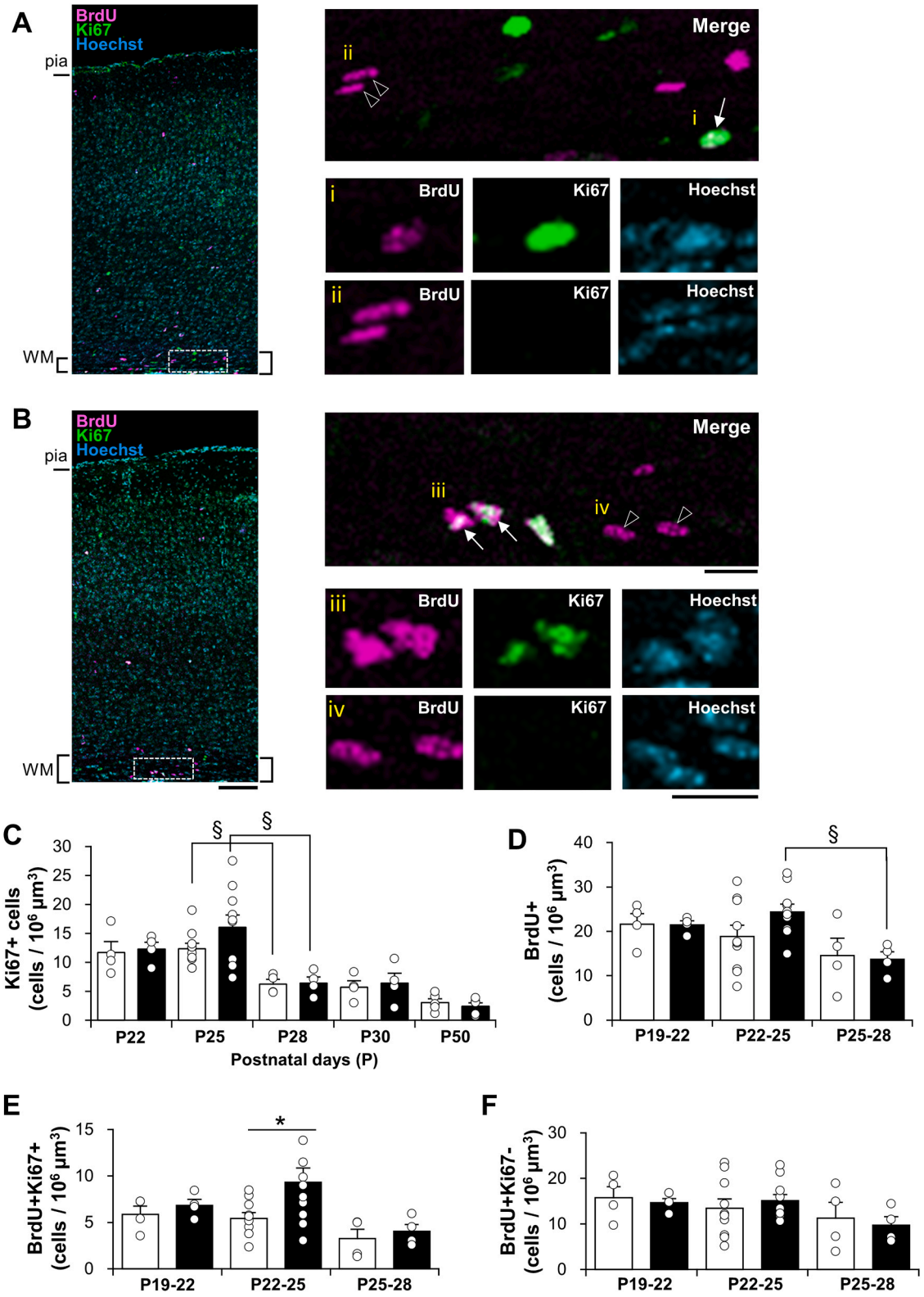

Fig. 2. Proliferative states of cells in the subcortical white matter during fourth postnatal week. A, B. Confocal immunofluorescence images of BrdU (magenta), Ki67 (green), and Hoechst (cyan) staining in V1b (left) and white matter (right) in control (A) and BE mice (B) on P25. BrdU+Ki67+ cells (arrow) and BrdU+Ki67- cells (arrowheads) are shown in magnified images below (i~iv). Scale bars, 100 µm (left), 50 µm (top right) and 20 µm (bottom right) for A and B. C. The time course of Ki67+ cell densities for control (□) and BE mice (■). D–F. The cell densities of BrdU+ (D), BrdU+Ki67+ (E), and BrdU+Ki67- (F) cells detected on P22, P25 and P28 after 4-day injections from P19 (P19–22), P22 (P22–25) and P25 (P25–28), respectively. In both control (□) and BE (■) mice, N = 4 for P19–22, N = 10 for P22–25, and N = 4 for P25–28. §$p < 0.05$, one-way ANOVA, Tukey-Kramer test. *$p < 0.05$, unpaired Student's *t*-test.

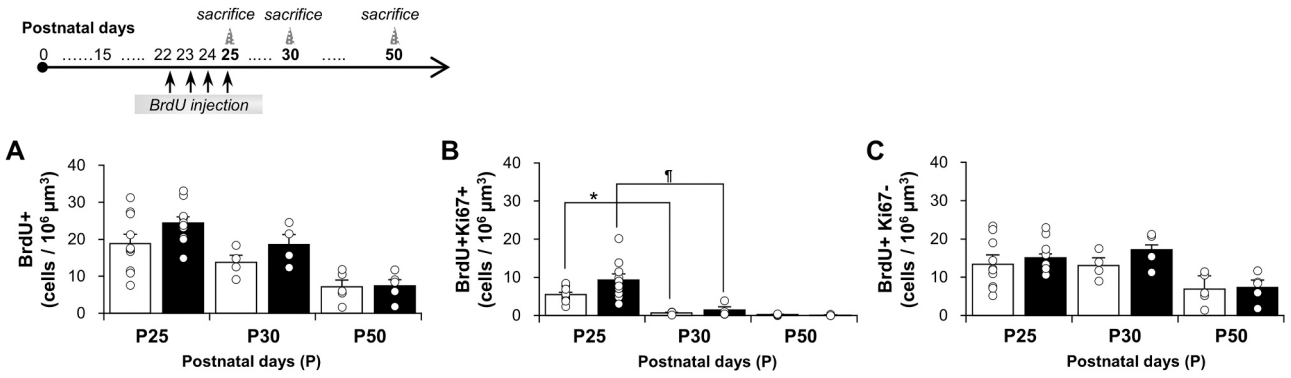

Fig. 3. Progression of P22–25 proliferated OPCs. A scheme of experimental time course. A–C. Cell densities of BrdU+ (A), BrdU+Ki67+ (B), BrdU+Ki67- (C) cells on P25, P30, and P50 after 4-day injections from P22 to P25. For control (□) and BE (■) mice, N = 5 for P25, N = 4 for P30, and N = 5 for P50. One-way ANOVA, *F(2, 16) = 28.78, p = 0.00012, ¶ F(2, 16) = 12.37, p = 0.0077.

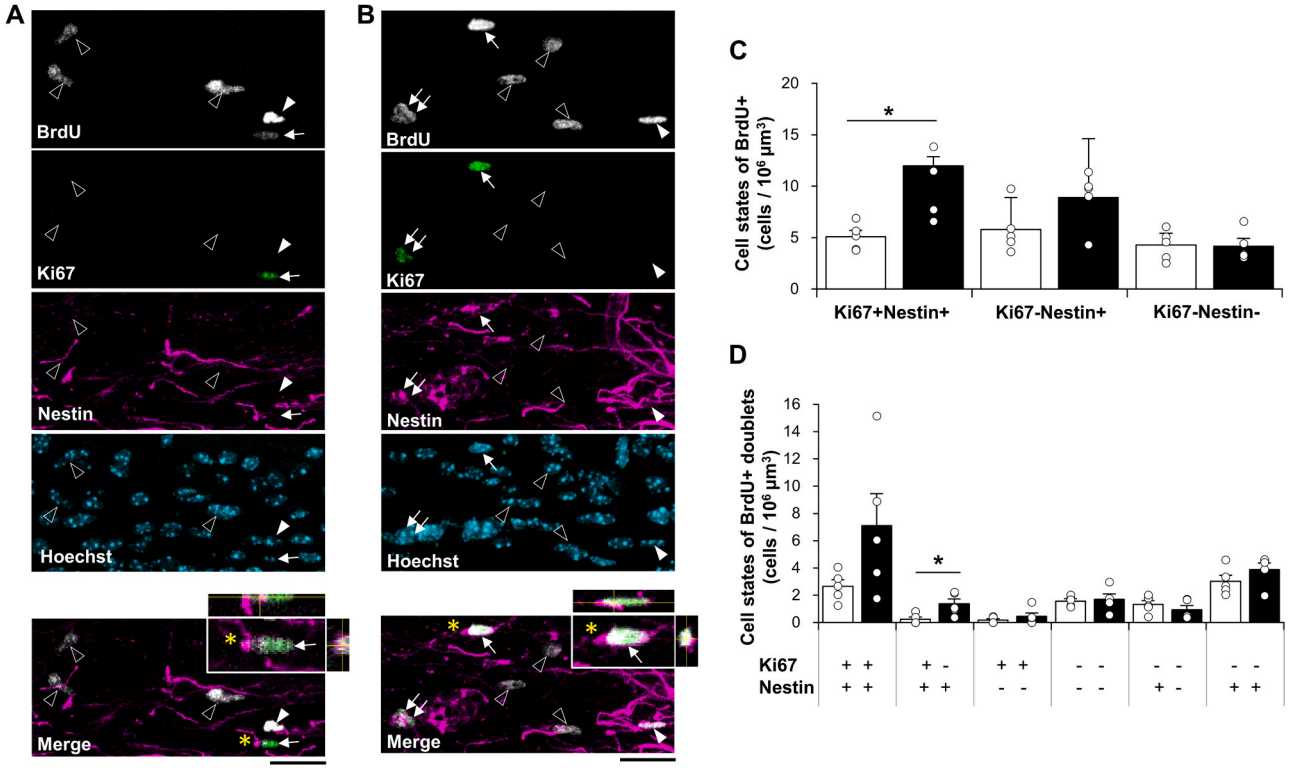

Fig. 4. Cell states of P22–25 proliferated OPCs. A, B. Representative confocal images showing P22–25 BrdU+ cells and staining for Ki67 and Nestin in the white matter of V1 in control (A) and BE (B) mice. Ki67+Nestin+ (arrow), Ki67-Nestin+ (closed arrowhead), and Ki67-Nestin- (open arrowhead) BrdU+ cells. BrdU+Ki67+Nestin+ cells (asterisks) are magnified to show the x-z and y-z cross-section views. Scale bars, 50 µm. C. Cell densities of BrdU+ cells expressing Ki67 and/or Nestin. *p < 0.05, one-way ANOVA, Tukey-Kramer test. N = 5 for both control (□) and BE (■) mice. D. Doublet analysis of BrdU+ cells for Ki67 and/or Nestin expression. *p < 0.05, one-way ANOVA, Tukey-Kramer test.

mode of OL-lineage progression. BE significantly elevated the cell densities of NG2+Nestin+ symmetric doublets, confirming the increase of OPCs as found above. Although lower in cell density, NG2-Nestin+ symmetric GPC doublets were also increased by BE (Fig. 5D). Other cell types were unaffected. These data suggest that BE promoted undifferentiated cell formation.

Next, we also tested if BE affected oligodendrocyte lineage of P22–25 BrdU+ cells by immunostaining against NG2, PDGFRα and CC1 (Fig. 5E–G). PDGFRα is expressed in OPCs, while CC1 is presumably expressed in late pre-OLs as well as maturing OLs (Fig. 5A, e.g., Nagy et al., 2017). Our analysis shows that BE appeared to increase NG2+PDGFRα+CC1- cells (OPCs), but no clear BE effects on NG2+PDGFRα-CC1- cells (early pre-OLs), NG2+PDGFRα-CC1+ cells (late pre-OLs) or NG2-PDGFRα-CC1+ cells (OLs) were found (Fig. 5F). The doublet cell density analysis indicated that BE increased symmetric OPCs (Fig. 5G). These data further support our contention that BE increases proliferative OPCs in the P22–25 proliferated cells.

BE effects on gliosis in the subcortical WM and the dorsal lateral geniculate nucleus (dLG)

The effects of BE on oligodendrocyte lineage cells might be due to structural or functional changes in the subcortical WM of V1. Previous studies have shown that BE at birth degenerated retinal nerves to dLG (Reese, 1986) and reduced its size (Heumann and Rabinowicz, 1980; Asanuma and Stanfield, 1990; Massé et al., 2014), potentially affecting

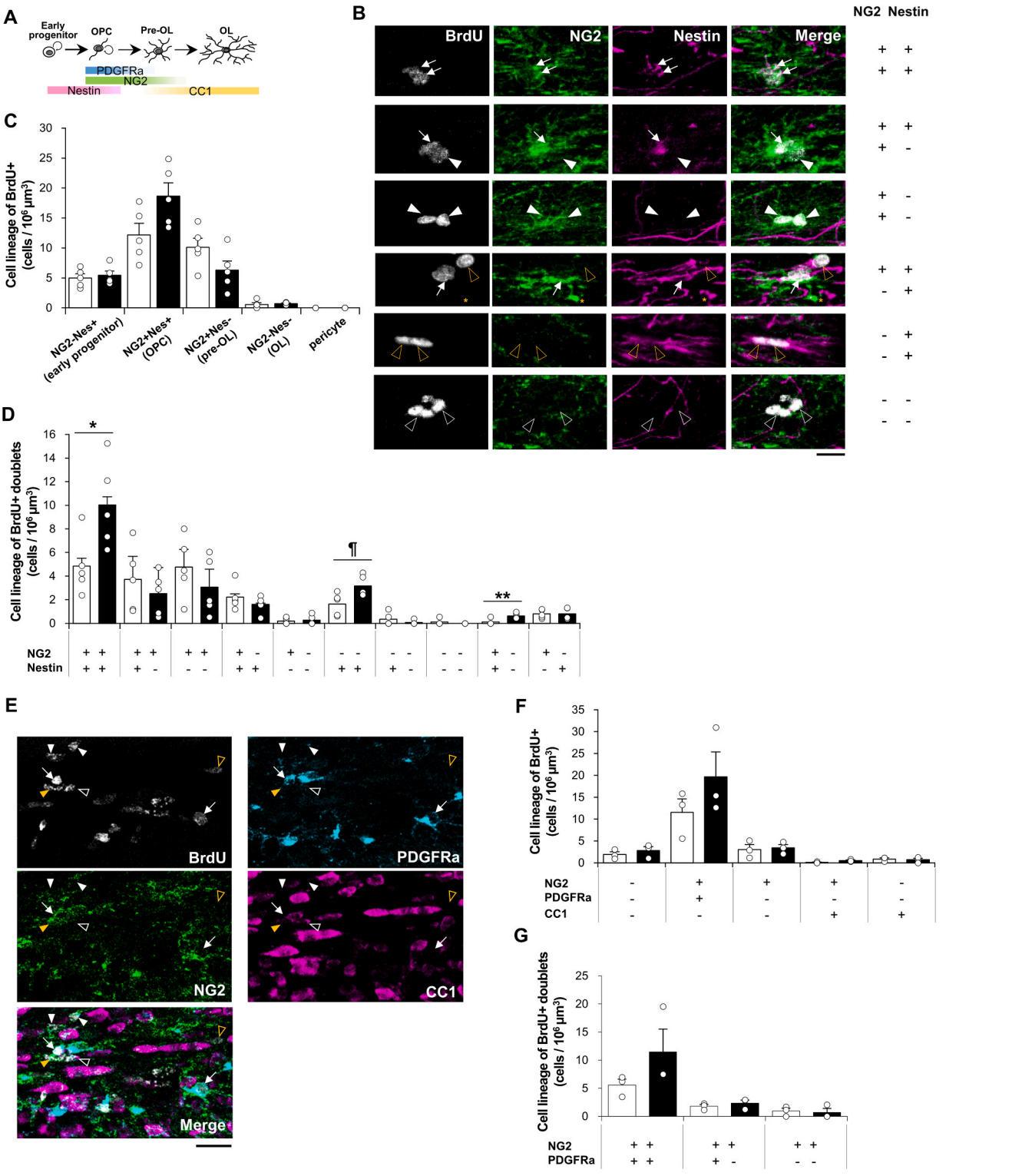

Fig. 5. Lineage progression of P22–25 proliferated cells. A. A scheme showing lineage progression of oligodendrocyte lineage cells and expression of Nestin, PDGFRα, NG2 and CC1 in each cell type. B. Representative images of BrdU+ (gray) sister cells stained for NG2 (green) and Nestin (magenta). Key on the right shows NG2 and Nestin expression in doublets. NG2+Nestin+ (white arrow), NG2+Nestin- (closed white arrowhead), NG2-Nestin+ (open yellow arrowhead), and NG2-Nestin- (open white arrowhead). A yellow asterisk indicates a NG2 and Nestin-colabeled pericyte. Scale bar, 20 µm. C. Cell densities of BrdU+ singlets. D. Cell densities of BrdU+ doublets. One-way ANOVA: *$F(1, 8) = 6.82$, $p = 0.031$ for NG2+/+Nestin+/+. ¶$F(1, 8) = 7.19$, $p = 0.028$ for NG2-/-Nestin+/+. **$F(1, 8) = 8.93$, $p = 0.017$ for NG2+Nestin+&NG2-Nestin-. E. Confocal images for BrdU (gray), PDGFRα (cyan), NG2 (green), CC1 (magenta), and overlaid (Merge) stains. PDGFRα-NG2-CC1- (yellow open arrowhead, early progenitor), PDGFRα+NG2+CC1- (white arrow, OPC), PDGFRα-NG2+CC1- (white closed arrowhead, early pre-OL), PDGFRα-NG2+CC1+ (yellow closed arrowhead, late pre-OL), PDGFRα-NG2-CC1+ (white open arrowhead, OL) BrdU+ cells. F. Single cell density analysis of BrdU+ cell types with PDGFRα, NG2 and/or CC1 expression on P25. G. Doublet analysis of BrdU+ cell types with PDGFRα and/or NG2 expression on P25. (For interpretation of the references to color in this figure legend, the reader is referred to the web version of this article.)

the structure and/or function of thalamocortical axons and resulting in the OPC changes in the subcortical WM. As a step toward understanding this possibility, we examined if injury is involved in the BE-induced OPC change. Since injury due to axonal degeneration and neuronal death would induce gliosis, we used GFAP upregulation as a marker of astrogliosis and CD68 as a marker of microglial phagocytic activity in the subcortical WM as well as in dLG (Fig. 6). No clear difference in the expression of the two markers was detected in the WM between control and BE mice (Fig. 6A, B). In dLG, however, GFAP expression was upregulated more in BE mice than in control mice, and some CD68+ cells were detected along the GFAP-labeled area in BE mice, but not in control mice (Fig. 6C, D; 2 sections/mouse, N = 3). These data suggest that the BE-induced OPC elevation is not likely due to injury in the V1 subcortical WM but could involve changes in dLG and consequent alteration of thalamocortical signaling.

BE effects on the destiny of P22-25 BrdU-labeled OPCs

We then examined if BE affected the destiny of P22–25 BrdU-labeled OPCs beyond P25. Tracing the BrdU+ cells at 5 and 25 days after the last BrdU injection showed that the proliferated cells declined similarly between control (~24%) and BE mice (~28%) from P25 to P30, but the cells decreased from P30 to P50 more in BE mice (~62%) than in control mice (~48%) (Fig. 3A). The BrdU+ cell densities were slightly higher in BE mice than in control mice on P30 as for P25 (but not significantly different, unpaired Student's *t*-test, $p = 0.45$), but they were similar between control and BE mice on P50 (unpaired Student's *t*-test, $p = 0.14$). Thus, the difference in the average values of the proliferated cells between control and BE mice were maintained until P30. To determine if it is the cycling cells or cell cycle-exited cells that decreased among the proliferated cells, we examined the destiny of BrdU+Ki67+ and BrdU+Ki67- cells.

The cell density of BrdU+Ki67+ cells that were elevated in BE mice almost disappeared fully on or before P30 as in control mice (Fig. 3B). The BrdU+Ki67+ cell densities further decreased to almost none at P50 in both control and BE mice (No BrdU+Ki67+ cells were found in 1 out of 5 control mice and 4 out of 5 BE mice.). In contrast, the cell densities of BrdU+Ki67- cells remained similar between P25 and P30 for both control and BE mice (Fig. 3C). These data suggest that it is the cycling, not the cell cycle-exited, BrdU+ cells that decreased from P25 to P30. Meanwhile, from P30 to P50, BrdU+Ki67- cell density decreased about 47%, while BrdU+Ki67+ cell densities at P30 were not different from those at P50. Thus, the decline of BrdU+ cell densities from P30 to P50 (Fig. 3A) is likely due to the disappearance of the BrdU+Ki67- differentiated cells. These results indicate that the P22–25 BrdU+ cells undergo their developmental disappearance via at least two different steps: the loss of BrdU+Ki67+ cells, followed by the loss of BrdU+Ki67- cells. It is unclear if the BrdU+Ki67+ cells themselves have directly disappeared, or if they transitioned first to BrdU+Ki67- cells, while a similar number of previously BrdU+Ki67- cells have disappeared.

Overall, in the subcortical WM of V1, P22–25 BrdU+ OPCs progressively decreased over 25 days in control mice. This decrease was largely due to the loss of proliferative cells for the first 5 days and followed by the loss of cell cycle-exited cells after P30. BE transiently upregulated a proliferative state of P22–25 BrdU+ OPCs at P25 but showed little effects on their destiny until P50.

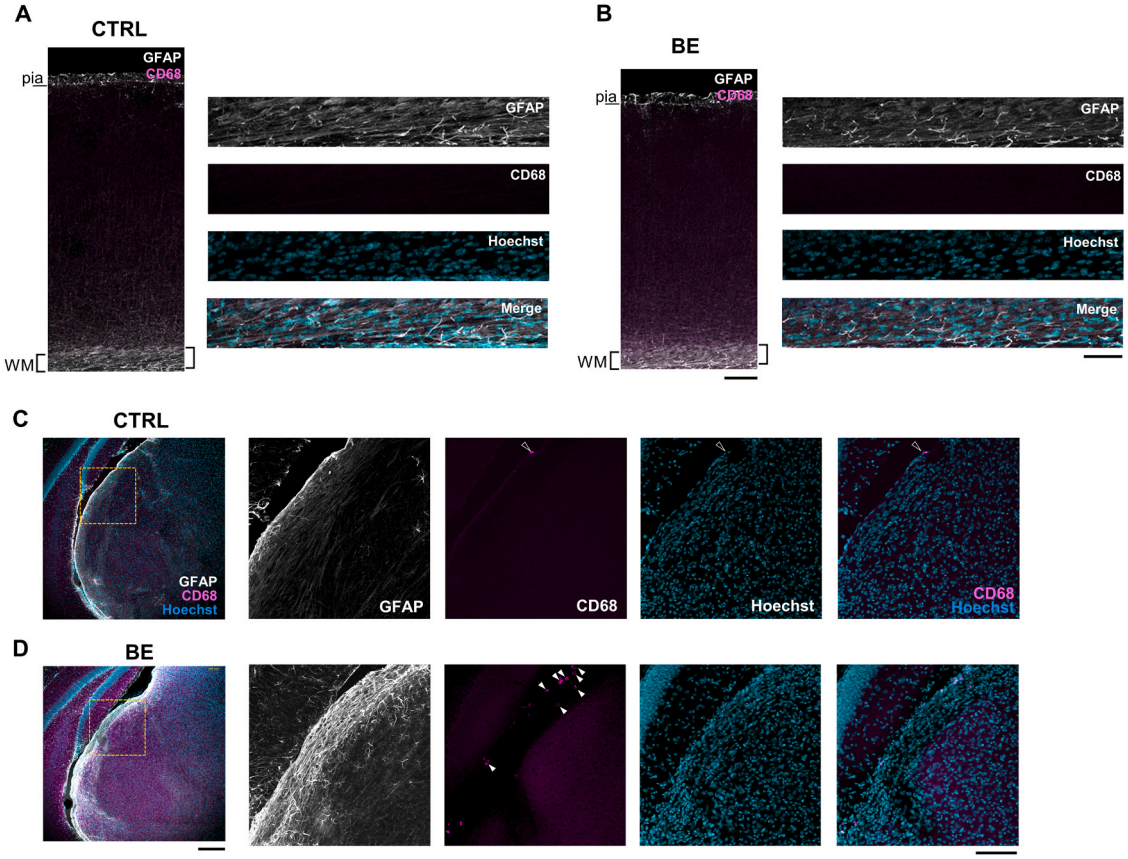

Fig. 6. Gliosis in V1 and the thalamus. A, B. Representative images of GFAP (gray) and CD68 (magenta) in V1b (left) and in the subcortical WM (right) with Hoechst (cyan) and overlaid stains (Merge) for control (CTRL, A) and BE mice (B). Scale bars, 100 μm (left), 50 μm (right). C, D. Representative images of GFAP (gray), CD68 (magenta), Hoechst (cyan) in the thalamus that contains MGv and dLG for control (CTRL, C) and BE (D) mice. Boxed region was magnified for dLG (right four images). CD68 and Hoechst images were merged to identify phagocytic microglia (white closed arrowheads). Non-specific stain in CTRL (white open arrowhead). Scale bars, 100 μm (left), 50 μm (right).

Maturation of P22-25 proliferated OPCs

The maturation of the P22–25 proliferated BrdU+ cells was then examined by an oligodendrocyte marker 2′,3′-Cyclic-nucleotide 3′-phosphodiesterase (CNPase). Immunofluorescent staining of BrdU and Olig2 along with CNPase showed that BrdU+ cells present within CNPase+ thick fibers in the WM were essentially all Olig2+ (Fig. 7; 100 ± 0% at P30, 96 ± 4% at P50). BrdU+Olig2+ cells expressing CNPase around the nucleus in the cytosol existed at a very low density (0.54 cells/10^6 μm^3) in control mice at P25 (Fig. 7A), which is consistent with the cell density of NG2-Nestin- cells (0.6 cells/10^6 μm^3; Fig. 4B). Its proportion among BrdU+Olig2+ cells was 0.3 ± 0.3%, indicating that very few BrdU+ cells became maturing OLs. At P30, more BrdU+ cells became maturing OLs (Fig. 7B) as they expressed CNPase in nearly one-

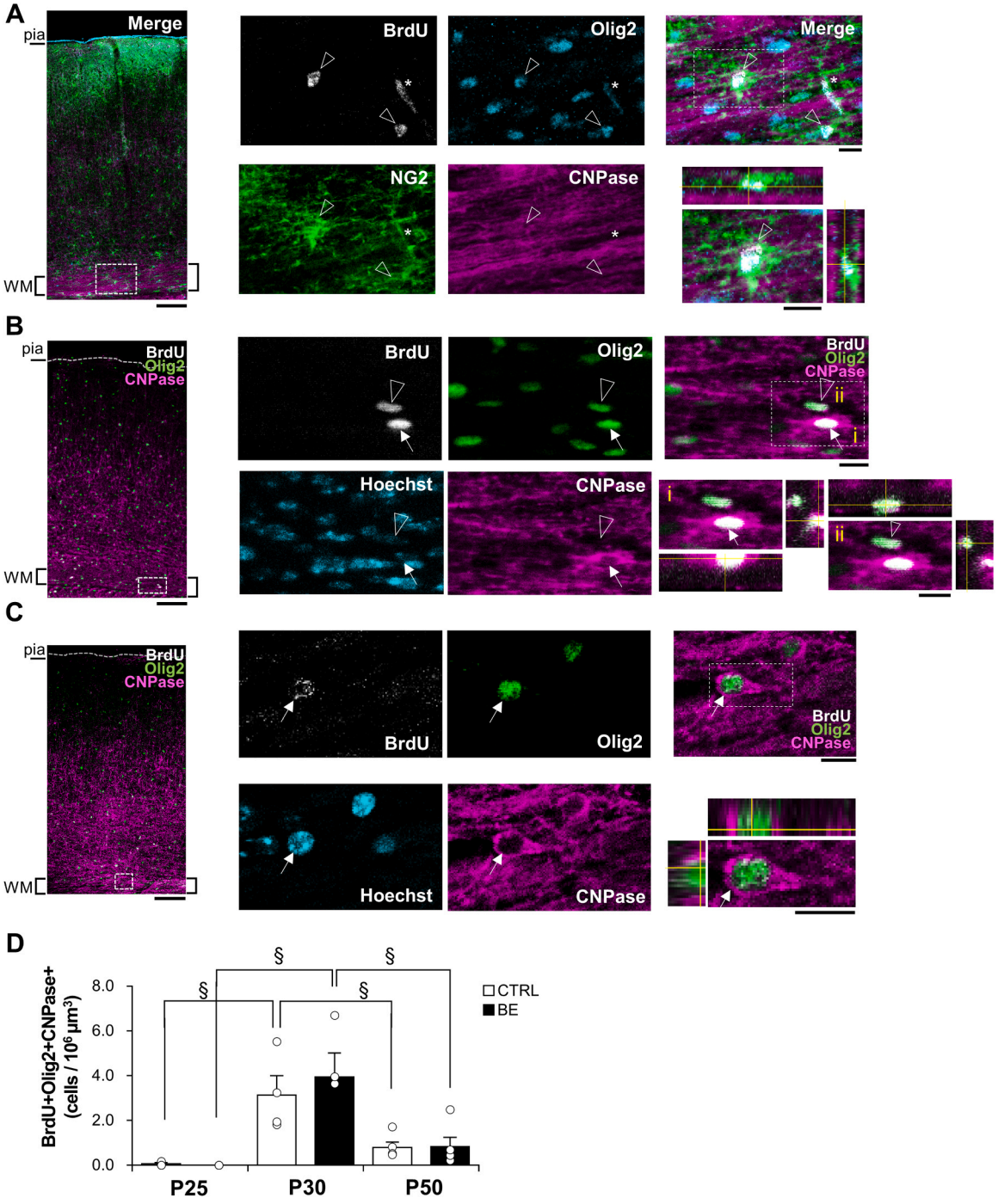

Fig. 7. Differentiation of P22–25 proliferated OPCs. A. Representative images of BrdU (gray), Olig2 (cyan), NG2 (green), CNPase (magenta), and overlaid for all four (Merge) in V1b (left) and in the WM on P25. A boxed area was magnified to show that NG2 surrounds Olig2, but CNPase is not expressed in the cytosol. Open arrowheads indicate BrdU+Olig2+NG2+CNPase- cells. The x-z and y-z cross-section views of the white boxed image are shown at the top and right side of the magnified image, respectively. Scale bars, 10 μm. B, B, C. Representative images in V1b (left) and in the WM (right) on P30 (B) and P50 (C). BrdU (gray), Olig2 (green), CNPase (magenta), Hoechst (cyan). BrdU+Olig2+CNPase+ cell (arrow) and BrdU+Olig2+CNPase- cell (open arrowhead) were magnified. Scale bars, 10 μm. D. Cell densities of maturing OLs on P25, P30, and P50 in CTRL (□) and BE (■) mice. N = 3 for P25, N = 4 for P30, N = 5 for P50. §$p < 0.05$, one-way ANOVA, Tukey-Kramer post-hoc tests.

fourth of the BrdU+Olig2+ cell population (25.6 ± 8.8%, N = 4). Since the proportion of BrdU+ cells that exited the cell cycle (i.e., Ki67-) was about 95% at P30, these results suggest most BrdU+ cells exited the cell cycle and transitioned to CNPase- presumptive pre-OLs or quiescent cells. BE did not significantly alter the cell density of BrdU+Olig2+CNPase+ OLs (Fig. 7D) nor their proportion among the BrdU+Olig2+ cells (27.1 ± 8.5% for BE, N = 4).

At P50, the cell density of BrdU+Olig2+CNPase+ OLs declined about 4-fold from P30 (Fig. 7D). This decline in maturing OLs of about 2.3 cells/10^6 μm^3 was less than the loss of BrdU+Ki67- cells of about 6.2 cells/10^6 μm^3 (Fig. 6C), suggesting that the disappearance of BrdU+ cells underlies the loss of maturing OLs, and that other cell cycle-exited cells were also lost during this period. Further, since most maturing OLs formed at P30 did not persist until P50, those cells that committed for maturation might undergo cell death. BE had little effects on the BrdU+Olig2+CNPase+ cell densities (Fig. 7D). The CNPase+ OLs constituted 33.6 ± 8.9% (N = 5) of BrdU+Olig2+ cells in control mice at P50. This proportion of maturing OLs was unchanged from P30 to P50 (unpaired Student's *t*-test, p = 0.54). Since BrdU+Ki67+ cells were almost all absent and essentially all BrdU+ cells have already exited the cell cycle by P30 (Fig. 3B), the unchanged maturing OL proportion suggests the disappearance of P22–25 BrdU+ cells in equal proportion for the CNPase+ maturing OLs and CNPase- pre-OLs or quiescent OPCs. BE had no significant effects on the proportion of CNPase+ cells among the BrdU+Olig2+ cells (51.1 ± 11.3% for BE; unpaired Student's *t*-test, p = 0.26). Overall, BE had little influence on the lineage progression of P22–25 proliferated oligodendrocyte lineage cells toward maturation from P30 to P50.

Discussion

The subcortical WM of V1 sustains visual function and is the site of passing axons of corticopetal as well as corticofugal projection neurons. Given that white matter properties may contribute to neuronal computation and cognitive function (Bullock et al., 2005; Petersen and Sporns, 2015), understanding developmental and experience-dependent structural plasticity in the visual pathway will be important. We report here that P22–25 is a developmentally unique period of OPC homeostasis during the fourth postnatal week in the subcortical WM of V1. Newly proliferated OPCs mostly exit the cell cycle, while those that remain proliferative disappear within a few days. BE transiently increased proliferative OPCs without much affecting the progression to differentiated cells during the period or maturation several days later.

Developmental fate changes of oligodendrocyte lineage cells in control mice

In this study, we confirmed the relatively efficient cell cycle exit of OPCs in the WM of V1 during the fourth postnatal week. Our BrdU injection experiments showed nearly 75% of BrdU+ cells have exited the cell cycle (i.e., Ki67-) already on the last day of the 4-day BrdU injection for any of the three 4-day periods, while the rest (~25%) remained proliferative (Fig. 2). This proportion of the proliferative cells is about twice the proportion of cycling Olig2-lineage cells in adult corpus callosum (Dimou et al., 2008; Rivers et al., 2008). The cell cycle-exited cells at P25 could be subdivided into differentiated cells and quiescent cells. Since nearly 70% of total P22–25 BrdU+ cells have exited the cell cycle and about 30% of them were differentiated on P25, nearly 40% of the cell cycle-exited cells became differentiated in 4 days. The proportion of OLs generated in 7 months (from P45 to P255) in adult corpus callosum is 20% or more of total OLs (Rivers et al., 2008), while much fewer percentage of OPCs were differentiated in adult optic nerves (~6.5% in 2 months from P120 to P185; Young et al., 2013). Thus, compared to the adult WM in other areas, differentiation toward mature OLs is more efficient in the subcortical WM of V1 during the fourth postnatal week, as have been reported previously (Reviewed in Bergles and Richardson, 2015; Nishiyama et al., 2021).

Another finding is that the loss of Ki67+ proliferative cells from P25 to P28 could be explained by reduced proliferation rates and the disappearance of proliferated cells. The proliferation rates decreased about 23% from P22–25 to P25–28, and nearly all 4-day generated BrdU+Ki67+ cells during P22–25 disappeared within 5 days. It appears that the fate of the P22–25 proliferated cells is decided within the proliferating days, as those that remained proliferative (~30%) disappeared after a few days of their birth. Since the cell cycle-exited BrdU+Ki67- cell density did not increase during this transition, the loss of the proliferative cells is likely due to the disappearance of BrdU+ cells, rather than differentiation. Possible reasons for the disappearance will include cell death, suboptimal antigen detection, or migration away from the analyzed region. The absence of cleaved Caspase-3 immunopositive cells (data not shown) suggests necrotic cell death with a caspase-independent manner (Raff, 1998; Zangemeister-Wittke and Simon, 2001), although apoptosis is still a possibility because of the short window of cleaved caspase-3 expression. Cell death could occur due to BrdU-induced loss of the nuclear envelope (Okuda et al., 2009). Lowered BrdU labeled cells due to cell division and the consequent lack of its detection will be possible. Alternatively, OPCs migrated away from the analyzed area in the adolescent period, although proliferative cells in the WM were non-migratory in the adult (Gensert and Goldman, 1996). Further studies would be necessary to understand the precise nature of the proliferative cell loss and fate determination mechanism during the fourth postnatal week.

We also found that maturing OLs increased without progressive proliferation and differentiation from P25 to P30. Based on the NG2 and nestin staining experiments, maturing OLs can be estimated to be about 18% of BrdU+ cells and about 30% of cell cycle-exited BrdU+ cells at this age (Fig. 5C). The CNPase+ maturing OLs of P22–25 BrdU+ cells increased to 3.0 cells/10^6 μm^3 after 5 days (Fig. 7D), while the cell cycle-exited BrdU+Ki67- cell densities remained unchanged from P25 to P30 (Fig. 3C). Thus, we speculate that there was a cell state shift to maturing OLs among the cell cycle-exited oligodendrocyte lineage cells, increasing from ~4% at P25 to ~23% at P30. At this point, it is unclear if the cell state shift occurred within cell cycle-exited cells, or proliferative OPCs exited the cell cycle to supply maturing OLs, while some of the cell cycle-exited cells disappeared due to cell death, keeping the same level of cell cycle-exited cell density.

Following the cell cycle exit at P30, maturing OLs declined about 78% at P50, suggesting that most of the BrdU+ maturing cells disappeared over 20 days. This contrasts with the continuous increase of OLs in the corpus callosum that arose from the subventricular zone (SVZ) during the first postnatal month (Levison et al., 1993; Zerlin et al., 1995) and later until adulthood (Levison et al., 1999; Dimou et al., 2008). Thus, these findings suggest distinct oligodendrocyte physiology between the corpus callosum and the subcortical WM in V1. A possible cause of the reduction of maturing OLs is cell death of cell cycle-exited cells as seen for the loss of BrdU+Ki67- cells (6.2 cells/10^6 μm^3) from P30 to P50. The BrdU+Ki67- cell density at P50 (6.9 cells/10^6 μm^3) was much higher than the remaining mature OLs (0.72 cells/10^6 μm^3) in control mice. Therefore, the majority of remaining BrdU+ cells (~90%) apparently continue existing as immature differentiated cells (pre-OLs or CNPase- immature OLs), unless differentiated cells could reverse lineage progression to quiescence.

Effects of binocular enucleation on oligodendrocyte lineage progression

The main finding of this study is that BE at the eye opening upregulated proliferative OPCs on P25 without affecting the maturational progression in P22–25 proliferated cells. The BE effects were not very strong but consistently observed using combinations of various cell lineage markers. Clearer BE effects were seen in the doublet analyses, where BE increased symmetrically formed proliferative OPCs. However, our data are limited by the temporally cross-sectional analysis and relies heavily on the success of immunostaining and lineage markers used.

Lineage tracing utilizing transgenic mice in the future will be important to better classify the cell types and track proliferation, differentiation, and migration of OPCs.

Underlying causes for the BE-induced upregulation of proliferative OPCs will include axonal activity changes and/or white matter injury in the subcortical WM. Our data for GFAP and CD68 expression might exclude the latter possibility. The gliosis detected in dLG, however, suggests that neuronal properties changed in dLG. Possibilities would include retinogeniculate axon degeneration (Reese, 1986) or reduced dLG size as seen in neonatally enucleated mice (Heumann and Rabinowicz, 1980; Asanuma and Stanfield, 1990; Massé et al., 2014). This study provides preliminary evidence for possible dLG degeneration following enucleation at the time of natural eye opening rather than at birth.

A reduced number of neurons or an altered activity will influence the thalamocortical axons projecting through the subcortical WM and may affect OPCs. Previous studies demonstrated neuronal activity or inactivity regulates the maturation of oligodendrocyte lineage cells in the white matter (Reviewed in Fields, 2008; Richardson et al., 2011; Bergles and Richardson, 2015; Káradóttir and Kuo, 2018). In the subcortical white matter (corpus callosum) of premotor cortex (M2) in adolescent mice, enhanced firing of action potentials in layer 5 projection neurons promoted proliferation and differentiation of OPCs, forming mature OLs and thicker myelin (Gibson et al., 2014). Axonal activation may be the basis for the enhancement of oligodendrogenesis, proliferation, and differentiation as observed in the motor cortex following motor skill learning (McKenzie et al., 2014; Xiao et al., 2016) and in other brain areas of mice raised in enriched environment (Okuda et al., 2009; Ehninger et al., 2011; Simon et al., 2011; Hughes et al., 2018). In the meantime, raising rats in reduced sensory-motor stimulation (i.e., impoverished environment) delayed the maturation of myelination in the visual cortex (Narducci et al., 2018). Thus, an increase or a decrease in neuronal activity directly controls oligodendrocyte lineage progression. Mechanistically, the enhanced activity-induced OPC proliferation in the central motor pathway depended on synaptic inputs to OPCs via glutamate (Káradóttir et al., 2005, 2008; Kukley et al., 2007; Ziskin et al., 2007) in unmyelinated parts of axons (Kukley et al., 2007; Tomassy et al., 2014). It is not known how neuronal activity loss affects the lineage progression in the WM. In the study of Narducci et al., the level of myelination in the gray matter was normalized to that in the subcortical WM of the visual cortex. Therefore, the effects of the impoverished condition on the WM are unknown. In addition to visual information through the central visual pathway, influences of non-visual inputs will need to be considered as V1 receives sensory information other than the visual information directly from non-visual cortices or indirectly via thalamic nuclei (Larsen et al., 2009).

Effects of visual deprivation on the subcortical WM

The subcortical WM of V1 would contain afferent axons mainly from dLG. In addition to the dLG atrophy due to retinal nerve degeneration discussed above, BE may affect the WM via dLG as it receives the heteromodal axonal input from inferior colliculus (IC) as demonstrated in anophthalmic mice (Piché et al., 2004; Laemle et al., 2006; Chabot et al., 2007, 2008). Since IC neurons project to the bottom layer of V1 (Laemle et al., 2006), their axons may cross the subcortical WM. In addition, the subcortical WM of sighted mouse V1 would contain afferent axons from other thalamic nuclei, including visual thalamus (lateral posterior nucleus, LP: Simmons et al., 1982; Garrett et al., 1992; Charbonneau et al., 2012; laterodorsal nucleus, LD: Charbonneau et al., 2012), non-visual thalamus (anteromedial nucleus; anteroventral nucleus; anterodorsal nucleus; posterior nucleus: Larsen et al., 2009; Charbonneau et al., 2012), and motor-related thalamus (ventral anterior nucleus, ventrolateral nucleus, ventromedial nucleus: Charbonneau et al., 2012 but see Larsen et al., 2009). Previous studies showed blind model-dependent differences in the thalamic projections. For example, stronger projections to V1 from the following thalamic nuclei have been reported compared to sighted C56BL/6 mice: LD in neonatally enucleated mice (Charbonneau et al., 2012), LD and LP in ZRDCT/An anophthalmic mice (Godement et al., 1979; Kaiserman-Abramof et al., 1980 but see Charbonneau et al., 2012 for LP), and thalamic nuclei that normally do not project to V1 such as auditory, somatosensory, motor, and limbic thalamic nuclei in Gnat$^{-/-}$ mice, which lack rod-mediated vision (Larsen et al., 2009). In addition to these afferent axons, the subcortical WM might also contain subcortical projection neurons, which may undergo structural and functional changes upon visual deprivation (Rhoades et al., 1985). BE may alter functions of afferent and/or efferent axons in the subcortical WM of V1 during P22–25, inducing the detected increase in proliferative OPCs. Although we have not found any BE effects on the number of P22–25 proliferated oligodendrocytes in this study, future studies may reveal yet unidentified structural or functional consequences of the OPC alteration.

CRediT authorship contribution statement

Hyeryun Shin: Formal analysis, Funding acquisition, Investigation, Methodology, Validation, Visualization, Original draft, Review & editing. **Hideki D. Kawai**: Conceptualization, Funding acquisition, Project administration, Supervision, Original draft, Review & editing.

Acknowledgements

We thank Dr. R. Watanabe for sharing materials of immunohistochemistry. We thank members of the Kawai laboratory for their invaluable discussion on experiments. This work was supported by JSPS Grants-in-Aid for Scientific Research (C) 23500402, 19K06947 (H.D.K), the Grants-in-Aid from Sasakawa Scientific Research, 28-411 (H.S.).

Conflicts of Interest

The authors declare no competing financial interests.

Ethical Statement

The authors certify that animal experiments were carried out in accordance with the National Institute of Health Guide for the Care and Use of Laboratory Animals (NIH Publications No. 80-23) revised 2011. The authors also certify that all animal experiments have been approved by the Animal Care and Use Committee of Soka University. The authors attest that all efforts were made to minimize the number of animals used and their suffering.

References

Aerts, J., Nys, J., Arckens, L., 2014. A highly reproducible and straightforward method to perform in vivo ocular enucleation in the mouse after eye opening. J. Vis. Exp. 92, 1–5. https://doi.org/10.3791/51936.

Asanuma, C., Stanfield, B.B., 1990. Induction of somatic sensory inputs to the lateral geniculate nucleus in congenitally blind mice and in phenotypically normal mice. Neuroscience 39, 533–545. https://doi.org/10.1016/0306-4522(90)90241-U.

Bergles, D.E., Richardson, W.D., 2015. Oligodendrocyte development and plasticity. Cold Spring Harb. Perspect. Biol. 8, 020453 https://doi.org/10.1101/cshperspect.a020453.

Boda, E., Di Maria, S., Rosa, P., Taylor, V., Abbracchio, M.P., Buffo, A., 2015. Early phenotypic asymmetry of sister oligodendrocyte progenitor cells after mitosis and its modulation by aging and extrinsic factors. Glia 63, 271–286. https://doi.org/10.1002/glia.22750.

Bullock, T.H., Bennett, M.V.L., Johnston, D., Josephson, R., Marder, E., Fields, R.D., 2005. Neuroscience. The neuron doctrine, redux. Science 310, 791–793. https://doi.org/10.1126/science.1114394.

Chabot, N., Charbonneau, V., Laramée, M.-E., Tremblay, R., Boire, D., Bronchti, G., 2008. Subcortical auditory input to the primary visual cortex in anophthalmic mice. Neurosci. Lett. 433, 129–134. https://doi.org/10.1016/j.neulet.2008.01.003.

Chabot, N., Robert, S., Tremblay, R., Miceli, D., Boire, D., Bronchti, G., 2007. Audition differently activates the visual system in neonatally enucleated mice compared with anophthalmic mutants. Eur. J. Neurosci. 26, 2334–2348. https://doi.org/10.1111/j.1460-9568.2007.05854.x.

Charbonneau, V., Laramée, M.E., Boucher, V., Bronchti, G., Boire, D., 2012. Cortical and subcortical projections to primary visual cortex in anophthalmic, enucleated and sighted mice. Eur. J. Neurosci. 36, 2949–2963. https://doi.org/10.1111/j.1460-9568.2012.08215.x.

Chen, Z., Li, X., Zhou, J., Yuan, B., Yu, B., Tong, D., Cheng, C., Shao, Y., Xia, S., Zhang, R., Lyu, J., Yu, X., Dong, C., Zhou, W.H., Qiu, Z., 2017. Accumulated quiescent neural stem cells in adult hippocampus of the mouse model for the MECP2 duplication syndrome. Sci. Rep. 7, 1–9. https://doi.org/10.1038/srep41701.

Dawson, M.R., Polito, A., Levine, J.M., Reynolds, R., 2003. NG2-expressing glial progenitor cells: an abundant and widespread population of cycling cells in the adult rat CNS. Mol. Cell. Neurosci. 24, 476–488. https://doi.org/10.1016/S1044-7431(03)00210-0.

Dimou, L., Gallo, V., 2015. NG2-glia and their functions in the central nervous system. Glia 63, 1429–1451. https://doi.org/10.1002/glia.22859.

Dimou, L., Simon, C., Kirchhoff, F., Takebayashi, H., Gotz, M., 2008. Progeny of Olig2-expressing progenitors in the gray and white matter of the adult mouse cerebral cortex. J. Neurosci. 28, 10434–10442. https://doi.org/10.1523/JNEUROSCI.2831-08.2008.

Ehninger, D., Wang, L.P., Klempin, F., Römer, B., Kettenmann, H., Kempermann, G., 2011. Enriched environment and physical activity reduce microglia and influence the fate of NG2 cells in the amygdala of adult mice. Cell Tissue Res. 345, 69–86. https://doi.org/10.1007/s00441-011-1200-z.

Fields, R.D., 2008. White matter in learning, cognition and psychiatric disorders. Trends Neurosci. 31, 361–370. https://doi.org/10.1016/j.tins.2008.04.001.

Franklin, K.B.J., Paxinos, G., 2008. The Mouse Brain in Stereotaxic Coordinates, Compact 3rd Edition: The Coronal Plates and Diagrams. Academic Press, Cambridge, MA.

Gallo, V., Armstrong, R.C., 1995. Developmental and growth factor-induced regulation of nestin in oligodendrocyte lineage cells. J. Neurosci. 15, 394–406. https://doi.org/10.1523/JNEUROSCI.15-01-00394.1995.

Garrett, B., Sørensen, J.C., Slomianka, L., 1992. Fluoro-Gold tracing of zinc-containing afferent connections in the mouse visual cortices. Anat. Embryol. 185, 451–459. https://doi.org/10.1007/BF00174083.

Gautier, H.O.B., Evans, K.A., Volbracht, K., James, R., Sitnikov, S., Lundgaard, I., James, F., Lao-Peregrin, C., Reynolds, R., Franklin, R.J.M., Káradóttir, R.T., 2015. Neuronal activity regulates remyelination via glutamate signalling to oligodendrocyte progenitors. Nat. Commun. 6, 1–15. ⟨http://www.nature.com/doifinder/10.1038/ncomms9518⟩.

Gensert, J.M., Goldman, J.E., 1996. In vivo characterization of endogenous proliferating cells in adult rat subcortical white matter. Glia 17, 39–51. https://doi.org/10.1002/(SICI)1098-1136(199605)17:1%3C39::AID-GLIA4%3E3.0.CO;2-2.

Gerdes, J., Lemke, H., Baisch, H., Wacker, H.H., Schwab, U., Stein, H., 1984. Cell cycle analysis of a cell proliferation-associated human nuclear antigen defined by the monoclonal antibody Ki-67. J. Immunol. 133, 1710–1715. ⟨http://www.jimmunol.org/content/133/4/1710⟩.

Ghoumari, A.M., Baulieu, E.E., Schumacher, M., 2005. Progesterone increases oligodendroglial cell proliferation in rat cerebellar slice cultures. Neuroscience 135, 47–58. https://doi.org/10.1016/j.neuroscience.2005.05.023.

Gibson, E.M., Purger, D., Mount, C.W., Goldstein, A.K., Lin, G.L., Wood, L.S., Inema, I., Miller, S.E., Bieri, G., Zuchero, J.B., Barres, B.A., Woo, P.J., Vogel, H., Monje, M., 2014. Neuronal activity promotes oligodendrogenesis and adaptive myelination in the mammalian brain. Science 344, 1252304. https://doi.org/10.1126/science.1252304.

Godement, P., Saillour, P., Imbert, M., 1979. Thalamic afferents to the visual cortex in congenitally anophthalmic mice. Neurosci. Lett. 13, 271–278. https://doi.org/10.1016/0304-3940(79)91506-4.

Guo, F., Joyce, M., McCauley, E., Bannerman, P., Pleasure, D., 2009. Early postnatal proteolipid promoter-expressing progenitors produce multilineage cells in vivo. J. Neurosci. 29, 7256–7270. https://doi.org/10.1523/JNEUROSCI.5653-08.2009.

Heumann, D., Rabinowicz, T., 1980. Postnatal development of the dorsal lateral geniculate nucleus in the normal and enucleated albino mouse. Exp. Brain Res. 38, 75–85. https://doi.org/10.1007/BF00237933.

Hill, R.A., Patel, K.D., Goncalves, C.M., Grutzendler, J., Nishiyama, A., 2014. Modulation of oligodendrocyte generation during a critical temporal window after NG2 cell division. Nat. Neurosci. 17, 1518–1527. https://doi.org/10.1038/nn.3815.

Hughes, E.G., Kang, S.H., Fukaya, M., Bergles, D.E., 2013. Oligodendrocyte progenitors balance growth with self-repulsion to achieve homeostasis in the adult brain. Nat. Neurosci. 16, 668–676. https://doi.org/10.1038/nn.3390.

Hughes, E.G., Orthmann-Murphy, J.L., Langseth, A.J., Bergles, D.E., 2018. Myelin remodeling through experience-dependent oligodendrogenesis in the adult somatosensory cortex. Nat. Neurosci. 21, 696–706. https://doi.org/10.1038/s41593-018-0121-5.

Kaiserman-Abramof, I.R., Graybiel, A.M., Nauta, W.J., 1980. The thalamic projection to cortical area 17 in a congenitally anophthalmic mouse strain. Neuroscience 5, 41–52. https://doi.org/10.1016/0306-4522(80)90069-X.

Kang, S.H., Fukaya, M., Yang, J.K., Rothstein, J.D., Bergles, D.E., 2010. NG2 + CNS glial progenitors remain committed to the oligodendrocyte lineage in postnatal life and following neurodegeneration. Neuron 68, 668–681. https://doi.org/10.1016/j.neuron.2010.09.009.

Káradóttir, R., Cavelier, P., Bergersen, L.H., Attwell, D., 2005. NMDA receptors are expressed in oligodendrocytes and activated in ischaemia. Nature 438, 1162–1166. https://doi.org/10.1038/nature04302.

Káradóttir, R., Hamilton, N.B., Bakiri, Y., Attwell, D., 2008. Spiking and nonspiking classes of oligodendrocyte precursor glia in CNS white matter. Nat. Neurosci. 11, 450–456. https://doi.org/10.1038/nn2060.

Káradóttir, R.T., Kuo, C.T., 2018. Neuronal activity-dependent control of postnatal neurogenesis and gliogenesis. Annu. Rev. Neurosci. 41, 139–161. https://doi.org/10.1146/annurev-neuro-072116-031054.

Karlen, S.J., Krubitzer, L., 2009. Effects of bilateral enucleation on the size of visual and nonvisual areas of the brain. Cereb. Cortex 19, 1360–1371. https://doi.org/10.1093/cercor/bhn176.

Kremer, D., Göttle, P., Hartung, H.P., Küry, P., 2016. Pushing forward: remyelination as the new frontier in CNS diseases. Trends Neurosci. 39, 246–263. https://doi.org/10.1016/j.tins.2016.02.004.

Kukley, M., Capetillo-Zarate, E., Dietrich, D., 2007. Vesicular glutamate release from axons in white matter. Nat. Neurosci. 10, 311–320. https://doi.org/10.1038/nn1850.

Laemle, L.K., Strominger, N.L., Carpenter, D.O., 2006. Cross-modal innervation of primary visual cortex by auditory fibers in congenitally anophthalmic mice. Neurosci. Lett. 396, 108–112. https://doi.org/10.1016/j.neulet.2005.11.020.

Larsen, D.D., Luu, J.D., Burns, M.E., Krubitzer, L., 2009. What are the effects of severe visual impairment on the cortical organization and connectivity of primary visual cortex? Front. Neuroanat. 3, 30. https://doi.org/10.3389/neuro.05.030.2009.

Lendahl, U., Zimmerman, L.B., McKay, R.D.G., 1990. CNS stem cells express a new class of intermediate filament protein. Cell 60, 585–595. https://doi.org/10.1016/0092-8674(90)90662-X.

Levison, S.W., Chuang, C., Abramson, B.J., Goldman, J.E., 1993. The migrational patterns and developmental fates of glial precursors in the rat subventricular zone are temporally regulated. Development 119, 611–622. https://doi.org/10.1242/dev.119.3.611%0A.

Levison, S.W., Young, G.M., Goldman, J.E., 1999. Cycling cells in the adult rat neocortex preferentially generate oligodendroglia. J. Neurosci. Res. 57, 435–446. https://doi.org/10.1002/(SICI)1097-4547(19990815)57:4%3C435::AID-JNR3%3E3.0.CO;2-L.

Li, Q., Brus-Ramer, M., Martin, J.H., McDonald, J.W., 2010. Electrical stimulation of the medullary pyramid promotes proliferation and differentiation of oligodendrocyte progenitor cells in the corticospinal tract of the adult rat. Neurosci. Lett. 479, 128–133. https://doi.org/10.1016/j.neulet.2010.05.043.

Mangin, J.M., Li, P., Scafidi, J., Gallo, V., 2012. Experience-dependent regulation of NG2 progenitors in the developing barrel cortex. Nat. Neurosci. 15, 1192–1194. https://doi.org/10.1038/nn.3190.

Massé, I.O., Guillemette, S., Laramée, M.-E., Bronchti, G., Boire, D., 2014. Strain differences of the effect of enucleation and anophthalmia on the size and growth of sensory cortices in mice. Brain Res. 1588, 113–126. https://doi.org/10.1016/j.brainres.2014.09.025.

McKenzie, I.A., Ohayon, D., Li, H., De Faria, J.P., Emery, B., Tohyama, K., Richardson, W. D., 2014. Motor skill learning requires active central myelination. Science 346, 318–322. https://doi.org/10.1126/science.1254960.

Miller, I., Min, M., Yang, C., Tian, C., Gookin, S., Carter, D., Spencer, S.L., 2018. Ki67 is a graded rather than a binary marker of proliferation versus quiescence. Cell Rep. 24, 1105–1112. https://doi.org/10.1016/j.celrep.2018.06.110.

Nagy, B., Hovhannisyan, A., Barzan, R., Chen, T.-R., Kukley, M., 2017. Different patterns of neuronal activity trigger distinct responses of oligodendrocyte precursor cells in the corpus callosum. PLoS Biol. 15 (8), 2001993 https://doi.org/10.1371/journal.pbio.2001993.

Narducci, R., Baroncelli, L., Sansevero, G., Begenisic, T., Prontera, C., Sale, A., Cenni, M. C., Berardi, N., Maffei, L., 2018. Early impoverished environment delays the maturation of cerebral cortex. Sci. Rep. 8, 1–15. https://doi.org/10.1038/s41598-018-19459-y.

Nishiyama, A., Shimizu, T., Sherafat, A., Richardson, W.D., 2021. Life-long oligodendrocyte development and plasticity. Semin. Cell Dev. Biol. https://doi.org/10.1016/j.semcdb.2021.02.004.

Nishiyama, A., Suzuki, R., Zhu, X., 2014. NG2 cells (polydendrocytes) in brain physiology and repair. Front. Neurosci. 8, 1–7. https://doi.org/10.3389/fnins.2014.00133.

Okuda, H., Tatsumi, K., Makinodan, M., Yamauchi, T., Kishimoto, T., Wanaka, A., 2009. Environmental enrichment stimulates progenitor cell proliferation in the amygdala. J. Neurosci. Res. 87, 3546–3553. https://doi.org/10.1002/jnr.22160.

Petersen, S.E., Sporns, O., 2015. Brain networks and cognitive architectures. Neuron 88, 207–219. https://doi.org/10.1016/j.neuron.2015.09.027.

Piché, M., Robert, S., Miceli, D., Bronchti, G., 2004. Environmental enrichment enhances auditory takeover of the occipital cortex in anophthalmic mice. Eur. J. Neurosci. 20, 3463–3472. https://doi.org/10.1111/j.1460-9568.2004.03823.x.

Rafalski, V.A., Ho, P.P., Brett, J.O., Ucar, D., Dugas, J.C., Pollina, E.A., Chow, L.M.L., Ibrahim, A., Baker, S.J., Barres, B.A., Steinman, L., Brunet, A., 2013. Expansion of oligodendrocyte progenitor cells following SIRT1 inactivation in the adult brain. Nat. Cell Biol. 15, 614–624. https://doi.org/10.1038/ncb2735.

Raff, M., 1998. Cell suicide for beginners. Nature 396, 119–122. https://doi.org/10.1038/24055.

Reese, B.E., 1986. The topography of expanded uncrossed retinal projections following neonatal enucleation of one eye: differing effects in dorsal lateral geniculate nucleus and superior colliculus. J. Comp. Neurol. 250, 8–32. https://doi.org/10.1002/cne.902500103.

Rhoades, R.W., Mooney, R.D., Fish, S.E., 1985. Subcortical projections of area 17 in the anophthalmic mouse. Brain Res. 349, 171–181. https://doi.org/10.1016/0165-3806(85)90141-5.

Richardson, W.D., Young, K.M., Tripathi, R.B., McKenzie, I., 2011. NG2-glia as multipotent neural stem cells: fact or fantasy? Neuron 70, 661–673. https://doi.org/10.1016/j.neuron.2011.05.013.

Rivers, L.E., Young, K.M., Rizzi, M., Jamen, F., Psachoulia, K., Wade, A., Kessaris, N., Richardson, W.D., 2008. PDGFRA/NG2 glia generate myelinating oligodendrocytes

and piriform projection neurons in adult mice. Nat. Neurosci. 11, 1392–1401. https://doi.org/10.1038/nn.2220.
Schumacher, M., Hussain, R., Gago, N., Oudinet, J.P., Mattern, C., Ghoumari, A.M., 2012. Progesterone synthesis in the nervous system: implications for myelination and myelin repair. Front. Neurosci. 6, 1–22. https://doi.org/10.3389/fnins.2012.00010.
Simmons, P.A., Lemmon, V., Pearlman, A.L., 1982. Afferent and efferent connections of the striate and extrastriate visual cortex of the normal and reeler mouse. J. Comp. Neurol. 211, 295–308. https://doi.org/10.1002/cne.902110308.
Simon, C., Götz, M., Dimou, L., 2011. Progenitors in the adult cerebral cortex: cell cycle properties and regulation by physiological stimuli and injury. Glia 59, 869–881. https://doi.org/10.1002/glia.21156.
Stevens, B., Porta, S., Haak, L.L., Gallo, V., Fields, R.D., 2002. Adenosine: a neuron-glial transmitter promoting myelination in the CNS in response to action potentials. Neuron 36, 855–868. https://doi.org/10.1016/S0896-6273(02)01067-X.
Tomassy, G.S., Berger, D.R., Chen, H.-H., Kasthuri, N., Hayworth, K.J., Vercelli, A., Seung, H.S., Lichtman, J.W., Arlotta, P., 2014. Distinct profiles of myelin distribution along single axons of pyramidal neurons in the neocortex. Science 344, 319–324. https://doi.org/10.1126/science.1249766.
Xiao, L., Ohayon, D., Mckenzie, I.A., Sinclair-Wilson, A., Wright, J.L., Fudge, A.D., Emery, B., Li, H., Richardson, W.D., 2016. Rapid production of new oligodendrocytes is required in the earliest stages of motor-skill learning. Nat. Neurosci. 19, 1210–1217. https://doi.org/10.1038/nn.4351.
Young, K.M., Psachoulia, K., Tripathi, R.B., Dunn, S.J., Cossell, L., Attwell, D., Tohyama, K., Richardson, W.D., 2013. Oligodendrocyte dynamics in the healthy adult CNS: evidence for myelin remodeling. Neuron 77, 873–885. https://doi.org/10.1016/j.neuron.2013.01.006.
Zangemeister-Wittke, U., Simon, H.U., 2001. Apoptosis - regulation and clinical implications. Cell Death Differ. 8, 537–544. https://doi.org/10.1038/sj.cdd.4400844.
Zerlin, M., Levison, S.W., Goldman, J.E., 1995. Early patterns of migration, morphogenesis, and intermediate filament expression of subventricular zone cells in the postnatal rat forebrain. J. Neurosci. 15, 7238–7249. https://doi.org/10.1523/JNEUROSCI.15-11-07238.1995.
Ziskin, J.L., Nishiyama, A., Rubio, M., Fukaya, M., Bergles, D.E., 2007. Vesicular release of glutamate from unmyelinated axons in white matter. Nat. Neurosci. 10, 321–330. https://doi.org/10.1038/nn1854.